metals

MDPI

Article

One Step Hydrothermal Synthesis of Magnesium Silicate Impregnated Palm Shell Waste Activated Carbon for Copper Ion Removal

Choe Earn Choong [1], Gooyong Lee [2,*], Min Jang [3], Chang Min Park [4] and Shaliza Ibrahim [1,*]

[1] Department of Civil Engineering, Faculty of Engineering, University of Malaya, Kuala Lumpur 50603, Malaysia; cce_@live.com
[2] Division of Policy Research, Green Technology Center, 173, Toegye-ro, Jung-gu, Seoul 04554, Korea
[3] Department of Environmental Engineering, Kwangwoon University, 20 Kwangwoon-Ro, Nowon-Gu, Seoul 01897, Korea; minjang@kw.ac.kr
[4] Department of Environmental Engineering, Kyungpook National University, 80 Daehak-ro, Buk-gu, Daegu 41566, Korea; cmpark@knu.ac.kr
* Correspondence: bluewater0703@gmail.com (G.L.); shaliza@um.edu.my (S.I.); Tel.: +1-803-210-5357 (G.L.); +60-3-7967-4458 (S.I.); Fax: +1-803-777-0670 (G.L.); +60-3-7967-4966 (S.I.)

Received: 31 August 2018; Accepted: 19 September 2018; Published: 21 September 2018

Abstract: Magnesium silicate impregnated onto palm-shell waste activated carbon (PPAC) underwent mild hydrothermal treatment under one-pot synthesis, designated as PPAC-MC. Various impregnation ratios from 25 to 300% of $MgSiO_3$ onto PPAC were tested. High levels of $MgSiO_3$ led to high Cu(II) adsorption capacity. A ratio of 1:1 (PPAC-MS 100) was considered optimum because of its chemical stability in solution. The maximum adsorption capacity of PPAC-MS 100 for Cu(II) obtained by isotherm experiments was 369 mg g^{-1}. The kinetic adsorption data fitted to pseudo-second-order model revealed as chemisorption. Increasing ionic strength reduced Cu(II) adsorption capacity due to the competition effect between Na^+ and Cu^{2+}. In addition, PPAC-MS 100 showed sufficient adsorption capacity for the removal of Zn(II), Al(III), Fe(II), Mn(II), and As(V), with adsorption capacities of 373 mg g^{-1}, 244 mg g^{-1}, 234 mg g^{-1}, 562 mg g^{-1}, 191 mg g^{-1}, respectively. Three regeneration studies were also conducted. PPAC-MS was characterized using Fourier Transformed Infrared (FTIR), X-Ray powder diffraction (XRD), X-ray photoelectron spectroscopy (XPS), and Field Emission Scanning Electron Microscope (FESEM). Overall, PPAC-MS 100 is a competitive adsorbent due to its high sorption capacity and sufficient regeneration rate, while remaining economical through the reuse of palm-shell waste materials.

Keywords: one-pot synthesis; palm shell waste activated carbon; magnesium silicate; adsorption; potential toxic metals

1. Introduction

Copper is essential to life, but high concentrations have toxic effects on the environment and living organisms [1]. In humans, it can cause the failure of the kidney and liver [2]. Copper is commonly found in abandoned mining areas, electroplating wastewater, and other extant water bodies. Potential toxic metals (PTMs) such as copper can accumulate in living organisms because they are not biodegradable [3]. Several copper mining-factories operating in Malaysia discharge about 30 times higher Cu(II) concentration than regulations allow (<0.2 mg L^{-1}) [4].

Conventional treatment methods including chemical precipitation [5], adsorption [6] and membrane separation [7] are widely applied to treat PTMs wastewater. Among these technologies, adsorption technology is a promising method due to its low maintenance cost and high efficiency [8–10].

However, the adsorption method suffers in terms of developing efficient adsorbents together with reduction of removal capacity in the complex situation, while competing with chemical components [11]. Therefore, it is necessary to develop efficient adsorbents which can be adapted to complex conditions with efficient binding capacity for not only single-type metal adsorption, but also complex PTMs compounds.

Porous materials have advantages in adsorption due to their higher surface area and the ability to bind functional group on the surface [12]. Activated carbon is a type of porous material which is widely used for micropollutant adsorption because of its high specific surface area, adequate pore structure, and fast kinetic adsorption [13,14]. A great deal of research has investigated micropollutant removal using modified activated carbon with amine groups [15,16], Fe_2O_3 impregnation [17,18], anionic surfactants [19,20] and others. However, commercial active carbon is expensive, thus, several studies have been conducted to find economical adsorbents such as bamboo [21,22], spent tea leaves [23], nut shell [24,25], sawdust [26], and cotton hull [27]. In this study, palm shell waste activated carbon (PPAC) was used, which is a cost-effective material [28].

The effectiveness of magnesium silicate ($MgSiO_3$) for PTMs removal was recently studied [29], and it was noted that $MgSiO_3$ has the capability for ion exchange between Mg(II) and positively charged metal ions. However, nano-sized materials do not have a practical implementation for wastewater treatment because of separation difficulty in the treatment system and insufficient assessment of the toxicity of nano-sized materials [30,31]. To improve metal removal efficiency and hydro conductivity, several studies have examined chemical coatings such as iron oxide [32], silica [33], manganese oxide [34], magnetite lanthanum oxide [28], and zinc chloride [35] on active carbon, which has hydrophobic characteristics toward metal ions. However, $MgSiO_3$ coated onto active carbon for PTMs removal has not been studied. The main aim of this study is to develop a simple and novel one-pot synthesis method for coating $MgSiO_3$ onto surface of palm shell waste activates carbon (PPAC) with mild hydrothermal treatment and to investigate the optimum impregnated weight ratio between $MgSiO_3$ and PPAC for Cu(II) removal. Fourier Transformed Infrareds (FTIR), X-Ray powder diffraction (XRD), X-ray photoelectron spectroscopy (XPS) and Field Emission Scanning Electron Microscope (FESEM) were used to determine its mechanisms and characteristics. The adsorption isotherm and kinetic of Cu(II) removal of PPAC-MS 100, PPAC-MS 50, PPAC-MS 25 and PPAC were determined. Additional objectives were to determine the influence of pH and ionic strength on Cu(II) adsorption and examine the reusability of absorbent with magnesium solution and hydrochloride acid. Moreover, the mechanism of copper removal was investigated using modified PPAC. Furthermore, potential toxic metals (PTMs) such as Zn(II), Al(III), Fe(II), Mn(II) and As(V) removal were also conducted to evaluate the adsorption performance of PPAC-MS through isotherm adsorption.

2. Materials and Methods

2.1. Materials

2.1.1. Preparation of Magnesium Silicate Impregnated on PPAC

PPAC (mesh size 200) activated by potassium hydroxide (KOH) was obtained from Bravo Green Sdn. Bhd., Kuala Lumpur, Malaysia. Sodium Chloride (NaCl, purity > 99.0%), Copper sulphate ($CuSO_4$, purity > 99.0%), silicon powder (SiO_2, purity > 99.0%), magnesium oxide (MgO, purity > 99.0%), methanol, zinc nitrate ($ZnNO_3$), iron sulphate ($FeSO_4$, purity > 99.0%), manganese sulphate ($MnSO_4$, purity > 99.0%), sodium hydroxide (NaOH, purity > 99.0%) and nitric acid (HNO_3 purity > 90.0%) were obtained from R&M chemical (Selangor, Malaysia). Aluminum sulphate hydrate ($Al_2(SO_4)_3$, purity > 99.99%) and sodium arsenate (Na_3AsO_4, purity > 99.99%) were purchased from Sigma. 4.64 g of MgO and 6.76 g of SiO_2 dissolved into 100 mL DI water were stirred continuously at 30 °C to obtain magnesium silicate gel. For each silicate gel, 3.3, 5.0, 6.7, 10.0, 20.0, and 40.0 g of PPAC, respectively, were add and stirred for 1 h at 150 rpm. The amounts of PPAC were calculated based on ratio (wt%) of ($MgO + SiO_2$)/PPAC. Therefore, the ratio represents 300, 200, 150, 100,

50, and 25 wt% of ($MgO + SiO_2$)/PPAC, assigned as PPAC-MS 300, PPAC-MS 200, PPAC-MS 150, PPAC-MS 100, PPAC-MS 50 and PPAC-MS 25. The impregnated product was transferred into a stainless-steel Teflon-lined autoclave and treated at 150 °C for 10 h. The resulting product was filtered through 0.45µm-pore Whatman filter paper and washed with distilled water several times. After washing, the final impregnated product was dried in an oven at 70 °C for 24 h [36].

2.1.2. Optimization on Impregnated Ratio of $MgSiO_3$ on PPAC

Examination of copper adsorption on PPAC-MS with impregnation ratios ranging from 0–300% were carried out to investigate the optimum ratio of $MgSiO_3$ impregnated on PPAC. The experiments were conducted using 5 mg of PPAC-MS with 500 mg L^{-1} (pH 4.5) of 50 mL Cu(II) solution under 150 rpm for 24 h using PPAC-MS 300, PPAC-MS 200, PPAC-MS 150, PPAC-MS 100, PPAC-MS 50 and PPAC-MS 25. After adsorption, the suspension was filtered using a 0.45 µm pore size syringe filter. Then, Cu(II) concentration was determined using inductively coupled plasma optical emission spectrometry analysis (ICP-OES, Optima 5300V, Perkin Elmer, Waltham, MA, USA).

2.2. Batch Experiments for Cu(II) Removal

2.2.1. Adsorption Isotherms

Adsorption isotherm explains the adsorption molecule on the surface of an absorbent. To compare the Cu(II) removal capacity for PPAC-MS 100, PPAC-MS 50, PPAC-MS 25 and PPAC, adsorption experiments were conducted at varying initial concentrations. Equilibrium isotherm experiments were conducted with 5 mg of adsorbents with 50 mL Cu(II) solution under 150 rpm for 24 h [37]. Cu(II) solutions with 50 mg L^{-1}, 100 mg L^{-1}, 200 mg L^{-1}, 300 mg L^{-1}, 400 mg L^{-1} and 500 mg L^{-1} were prepared and the initial solutions were adjusted to pH 4.5 using 0.1 M Sodium Hydroxide (NaOH) and 0.1 M hydrochloric acid (HCl). After the isotherm experiments, the suspensions were filtered using 0.45 um pore size Whatman filter papers and Cu(II) concentrations were determined using ICP-OES analysis as per ASTM D1967-18 [38].

Values for q_e were calculated as follows [39]:

$$q_e = \frac{(C_o - C_e)V}{M} \tag{1}$$

where q_e is the adsorption capacity of solute absorbed at equilibrium (mg g^{-1}), C_e is the equilibrium concentration (mg L^{-1}), initial solution concentration (mg L^{-1}), M is the mass of absorbent (g) and V is the volume of solution (L). The isotherm data experiments were fitted to the Langmuir and Freundlich isotherms models.

The linear form of the Langmuir model is derived as follows [19]:

$$\frac{C_e}{q_e} = \frac{1}{Q_{\max} K_L} + \frac{C_e}{q_e} \tag{2}$$

where $Q_{\max}$ is the maximum adsorption capacity (mg g^{-1}) and K_L (L mg^{-1}) is the Langmuir constant related to the energy of adsorption. When adsorption is performed using a monolayer and uniform surface, the Langmuir model fits the isotherm data. Maximum adsorption capacity was achieved when all sorption sites were saturated. The linear form of Freundlich isotherm was calculated as follows [40]:

$$\log q_{eq} = \log K_F + \frac{1}{n} \log C_{eq} \tag{3}$$

where K_F and n are Freundlich isotherm constants related to adsorption capacity and adsorption intensity, respectively.

2.2.2. Adsorption Kinetics with Ionic Strength Effect

Kinetic adsorption experiments were conducted with 5 mg of absorbent with 50 mL of pollutant at 150 rpm at room temperature. 0 M, 0.01 M and 0.1 M NaCl with 500 mg L^{-1} of Cu(II) solution at pH 4.5 were prepared to investigate the influence of ionic strength on Cu(II) removal. Samples were collected at 30, 60, 90, 120, 150 and 180 minutes and analyzed for Cu(II) concentration. To analyze the kinetic adsorption process, the pseudo-first and pseudo-second order kinetics models were used. The pseudo first-order kinetic model is expressed as follows [25]:

$$\log (q_e - q_t) = \log q_e - \frac{K_1}{2.303} t \quad (4)$$

The pseudo second-order kinetic model is expressed as:

$$\frac{t}{q_t} = \frac{1}{K_2 {q_e}^2} + \frac{t}{q_e} \quad (5)$$

where q_e (mg g^{-1}) is the adsorption capacity at equilibrium, q_t (mg g^{-1}) is the amount of solute absorbed at time t, and K_1 (min^{-1}) and K_2 (g mg^{-1} min^{-1}) are the reaction rate constants for the pseudo first-order and pseudo second-order kinetic models, respectively.

2.2.3. pH Effect on PPAC-MS-100 for Cu(II) Removal

Adsorption experiments were carried out to determine the influence of pH on copper removal for PPAC-MS 100. 100 mg L^{-1} of Cu(II) solution was prepared and the initial pH levels were adjusted to 2, 3, 4, 5, 6 using 0.1 M of NaOH and 0.1 M of HCl. Adsorption experiments were conducted with 5 mg of absorbent with 50 mL of Cu(II) solution under 150 rpm for 24 h at room temperature. Samples were filtered through 0.45 µm pore size of Whatman filter and underwent ICP-OES analysis for Cu(II) concentration tracing.

2.2.4. Regeneration of PPAC-MS 100 for Cu(II) Adsorption

Three cycles of regeneration were performed to investigate the reusability of PPAC-MS 100 for Cu(II) removal. 5 mg of PPAC-MS 100 was added to a 50 mL solution containing 400 mg L^{-1} of Cu(II) in pH 4.5 and shaken at 150 rpm for 24 h. After adsorption, the suspensions were filtered and treated with 50 mg L^{-1} of Mg(II) solution or 0.1 M HCl solution, shaken under 150 rpm for 1 h at room temperature. The absorbent was washed several times with distilled water and dried in an oven at 70 °C for another adsorption cycle.

2.3. Adsorption Study of Dissociated PTMs by PPAC-MS 100

Langmuir and Freundlich isotherm modelling has been used to investigate adsorption capacities of PPAC-MS 100 to 5 types of different PTMs. 5 mg of PPAC-MS 100 were added to the solution: Zn(II) from 50 to 600 mg L^{-1}, Al(III) 50–500 mg L^{-1}, Fe(II) from 50 to 600 mg L^{-1}, Mn(II) from 50–500 mg L^{-1} and As(V) from 25 to 400 mg L^{-1}. 5 mg of PPAC-MS 100 was placed in 50 mL centrifuge tube at 150 rpm for 24 h at room temperature. The initial pH of the solution was not adjusted. After the suspension was filtered, the concentration of the pollutant was determined using ICP-OES.

2.4. Material Characterization

Surface functionalize groups were determined via Fourier Transformed Infrareds (FTIR) spectroscopy with a scanning range of 450 cm^{-1} to 4000 cm^{-1}. The characteristic textural structures of the pores of PPAC-MS 100, PPAC-MS 50, PPAC-MS 25 and PPAC were determined using a nitrogen gas adsorption analyzer (Mircrmeritics ASAP2020, Tristar II 3020, Norcross, GA, USA) to measure surface area, pore volume, and pore size distribution with relative pressure from range 0 to 1 p/p^o. Pore size distribution was calculated with Brunauer-Emmett-Teller (BET) and Barrett Joyner-Halenda (BJH)

equation. Moreover, the surface area was determined by Langmuir, BET and BJH equation. The surface morphologies of PPAC and PPAC-MS were determined with a Field Emission Scanning Electron Microscope (FESEM-EDX) (FEG Quanta 450, TSS Microscopy, Beaverton, OR, USA), EDX-OXFORD instrument (Abingdon, UK) and Hitachi SU8010 (Ibaraki, Japan). An X-Ray powder diffraction (XRD) pattern was obtained using X-Ray Diffractometers (Empyrean, Malvern Panalytical, Royston, UK) with an operational voltage of 40 kV and 40 mA current and Cu Kα radiation (λ). The XRD data was recorded in the range of 10–80° at 0.02 step size. The XRD raw data was evaluated using Highscore software (Plus version, Malvern Panalytical, Royston, UK). X-ray photoelectron spectroscopy (XPS) measurements were performed with ULVAC-PHI Quantera II using Al-Kα radiation (1486.6 eV) operated at 15 kV.

3. Results and Discussion

3.1. Optimization on Impregnated Ratio of $MgSiO_3$ on PPAC

To determine optimum ratio between $MgSiO_3$ and PPAC, several weight ratios of $MgSiO_3$/PPAC (0, 25, 50, 100, 150, 200 and 300 wt%, of $MgSiO_3$ impregnated onto PPAC) were tested for Cu(II) removal. The results for effect of impregnation ratio on Cu(II) removal is illustrated in Figure 1. In Figure 1, it is clear that impregnation ratio and Cu(II) removal capacity promoted a direct proportional relationship, the experimental results indicated that increasing impregnation ratio will also increase Cu(II) removal capacity. The highest impregnation ratio shows the highest Cu(II) removal capacity. The main removal mechanisms were adsorption and precipitation, as verified through FTIR, FESEM-EDX, XRD, and XPS (see details in Section 3.7 Material Characteristics). Material synthesis difficulty was encountered when the impregnation ratio went beyond 300% due to segregation between PPAC and excess $MgSiO_3$ gel. Moreover, the gradient in the Figure 1 curve decreases from 2.096 to 0.684 when the impregnation ratio is over 100%. Experimental results indicate that Cu(II) removal capacity had fewer increments when the impregnation ratio was greater than 100% due to the limitation of impregnation area on PPAC. Furthermore, $MgSiO_3$ leached from the PPAC-MS when the impregnation ratio was higher than 100%. Therefore, the following examination of Cu(II) adsorption will focus on 0–100% of $MgSiO_3$ impregnation ratio.

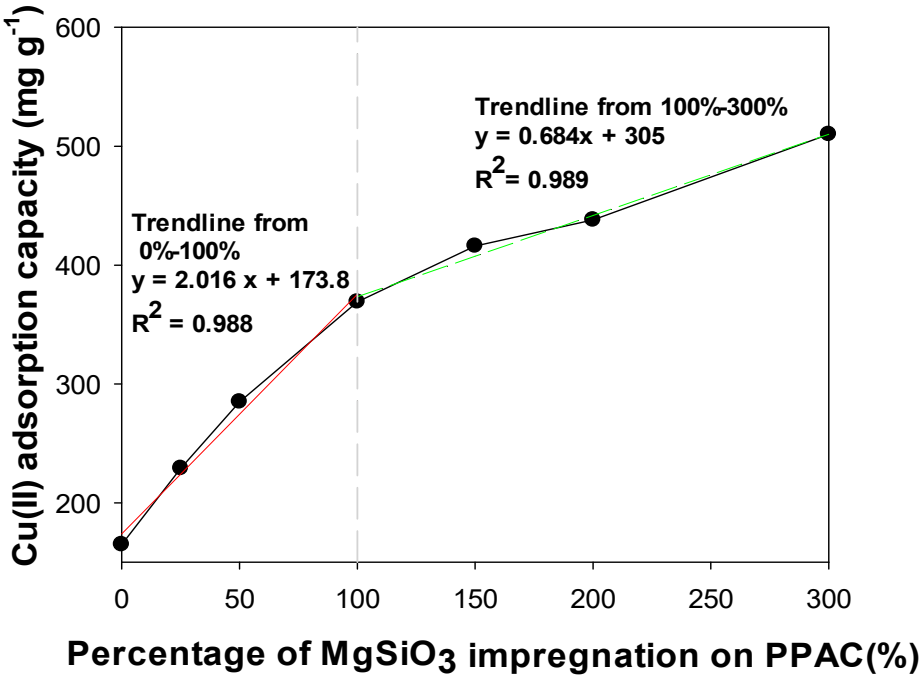

Figure 1. Adsorption isotherms of Cu(II) by different impregnation ratio of $MgSiO_3$ on PPAC.

3.2. Adsorption Isotherms for Cu(II)

Cu(II) adsorption values for PPAC-MS 100, PPAC-MS50, PPAC-MS 25 and PPAC were fitted to Langmuir and Freundlich isotherm model to describe the interactive behavior between absorbent and pollutant. Figure 2 compares the Langmuir and Freundlich isotherm curves for PPAC-MS 100, PPAC-MS 50, PPAC-MS25 and PPAC. Table S1 displays the adsorption isotherm parameters. The adsorption capacities from the experiment for Cu(II) removal were 369 mg g^{-1} for PPAC-MS 100, 285 mg g^{-1} for PPAC-MS50, 220 mg g^{-1} for PPAC-25, and 165 mg g^{-1} for PPAC. Isotherm results show that increasing impregnation ratios of $MgSiO_3$ result in the release of Mg^{2+} and OH^- release and an increase of Cu(II) removal capacity. Initial working solution prepared in pH 4.5 and the solution pH increased to pH 7–8 after Cu(II) isotherm adsorption experiments. This reveals that $MgSiO_3$ plays an important role in Cu(II) removal capacity. Thus, PPAC-MS 100 showed the highest Cu(II) removal capacity compared to PPAC-MS 50, PPAC-MS 25 and PPAC because it had the highest $MgSiO_3$ impregnation ratio. Compared to the other absorbent media (Table S2 in SI), PPAC-MS 100 showed high Cu(II) adsorption capacity except powdered MgO [41]. Although many factors contribute to adsorption performance, including surface area and impregnation compound on based material [42–44], it is clear that granular adsorbent has greater practical implementation for water treatment, but the available sorption area is lower than nano-particles [45]. Furthermore, because KOH has high efficiency for PTMs adsorption, PPAC activated by KOH may enhance Cu(II) removal.

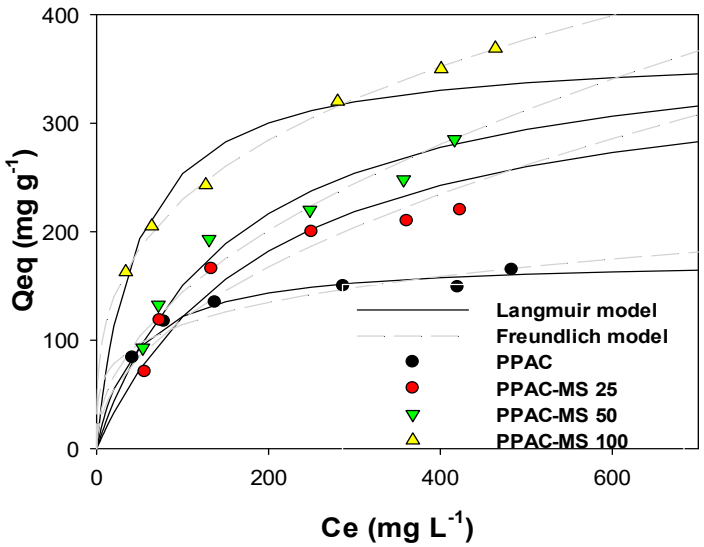

Figure 2. Adsorption isotherms of Cu(II) on PPAC and PPAC-MS 25, PPAC-MS 50 and PPAC-MS 100 with Langmuir modeling and Freundlich modeling.

According to the coefficient of determination (R^2) in Table S1, the adsorption of Cu(II) by PPAC-MS 50, PPAC-MS 25 and PPAC fitted well to Langmuir isotherm while PPAC-MS-100 fitted better with Freundlich isotherm. Theoretically, the Langmuir model is suitable for monolayer adsorption on homogenous surfaces [46], whereas the Freundlich model assumes the multilayer adsorption on heterogeneous surfaces [47]. The Langmuir isotherm model suggests the monolayer coverage of Cu(II) binding onto PPAC-MS 50, PPAC-MS 25 and PPAC surface homogeneously, while heterogeneous adsorption occurs on the PPAC-MS 100 surface with multiplayer coverage of Cu(II). Moreover, for the Freundlich isotherm constant, the n values presented in Table S1 for PPAC-MS 100 above describe the favorability of Cu(II) adsorption [41,48].

3.3. Adsorption Kinetics with Different Ionic Strength

Examination of kinetic adsorption studies were carried out using PPAC-MS 100, PPAC-MS 50, PPAC-MS 25 and PPAC with different ionic strengths of 0 M, 0.01 M, and 0.1 M NaCl. The kinetic

experiment results were fitted into pseudo first order modeling and pseudo-second-order modeling, as illustrated in Figure 3. Kinetic constants for pseudo first-order and second-order are summarized in Table S3. The kinetic experiment data was fitted using pseudo second-order modeling, with R^2 from 0.972 to 0.996. Furthermore, the kinetic results indicate that the overall adsorption process is closer to the chemisorptions process than the physisorption process [49], meaning that $MgSiO_3$ may be a main component for Cu(II) adsorption rather than PPAC.

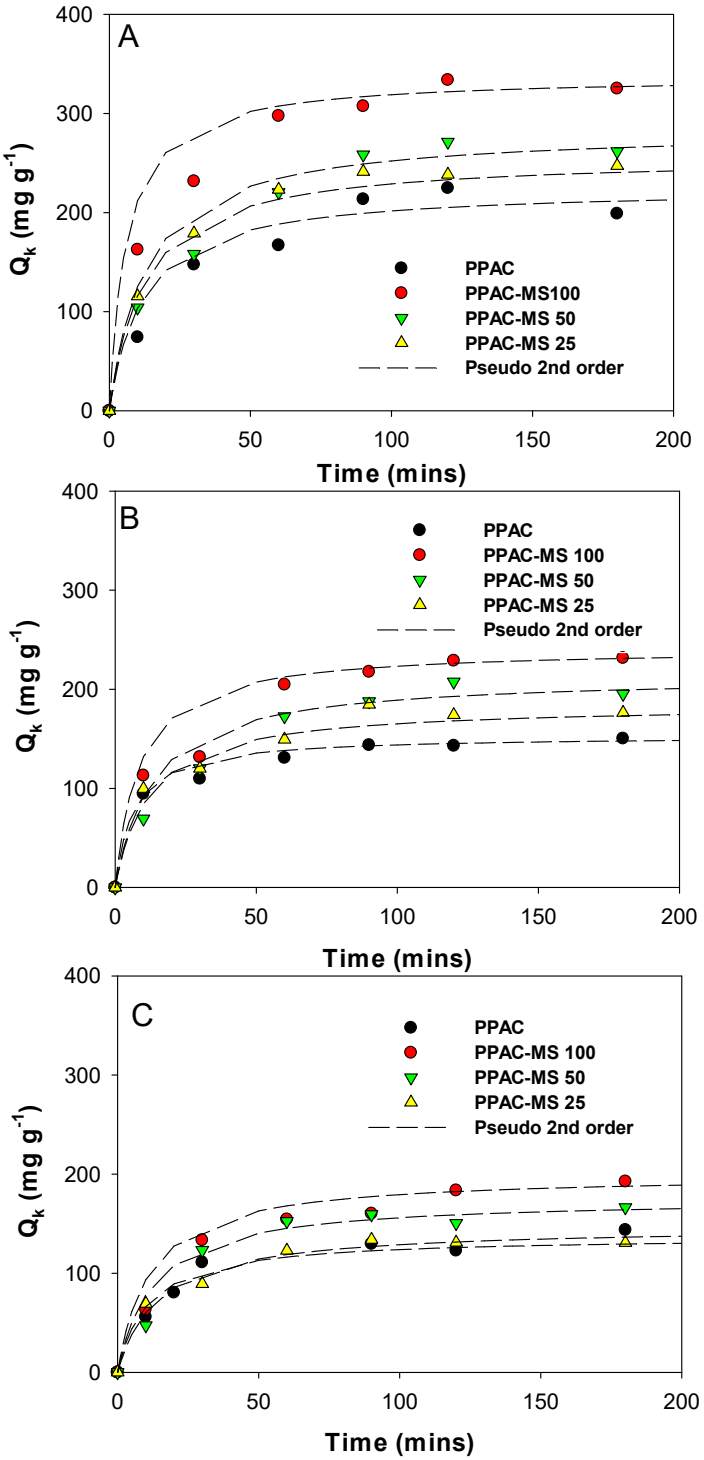

Figure 3. Effects of ionic strength on adsorption kinetics of Cu(II) by PPAC, PPAC-MS 100, PPAC-MS 50 and PPAC-MS 25 (**A**) no NaCl added, (**B**) 0.01 M NaCl and (**C**) 0.1 M NaCl.

As shown in Figure 3, ionic strength significantly influences the adsorption capacity of Cu(II). In terms of varying ionic strength conditions, Cu(II) removal capacity decreases when ionic strength increases. This phenomenon can be explained by the positively charged sodium ion contributing repulsive force at the outer layer of the absorbent and repelling positively charged copper ion [50]. Therefore, the available sorption surface decreases, resulting in a decrease of Cu(II) adsorption capacity.

Moreover, the adsorption reached equilibrium at 60 min for all absorbents at 0 M, 0.01 M and 0.1 M ionic strengths. It was found that higher ionic strength concentrations can increase the adsorption equilibrium rate. This phenomena can be explained by the competitive effect between the Cu(II) and Na^+ to compete for available adsorption site [51]. The adsorption rate may increase when the ionic strength increases.

3.4. Influence of pH on Cu(II) Removal Using PPAC-MS100

The influence of the pH value on Cu(II) adsorption capacity by PPAC-MS 100 was investigated in a range of pH 2–6, as shown in Figure 4. The Cu(II) adsorption capacity increases when the pH of initial solution increased. It can be explained that the PPAC-MS surface tends to be protonated by hydrogen ion (H^+) which promoted the competition between H^+ and Cu(II) at low pH. Al-Homaindan et al. (2014) have also explained that the reduction of metal sorption could be a result of the available sorption area for metal being occupied by proton in low pH. Therefore, adsorption capacity for Cu(II) was reduced at pH 2 because hydrogen ions (H^+) tend to compete with positively charged copper ions in solution. However, high initial solution might lead to metal ion precipitation to form insoluble salts because of the low amount of proton and high amount of OH^- ion [52]. Therefore, Cu(II) removal capacity increases with an increase in the pH of the initial solution.

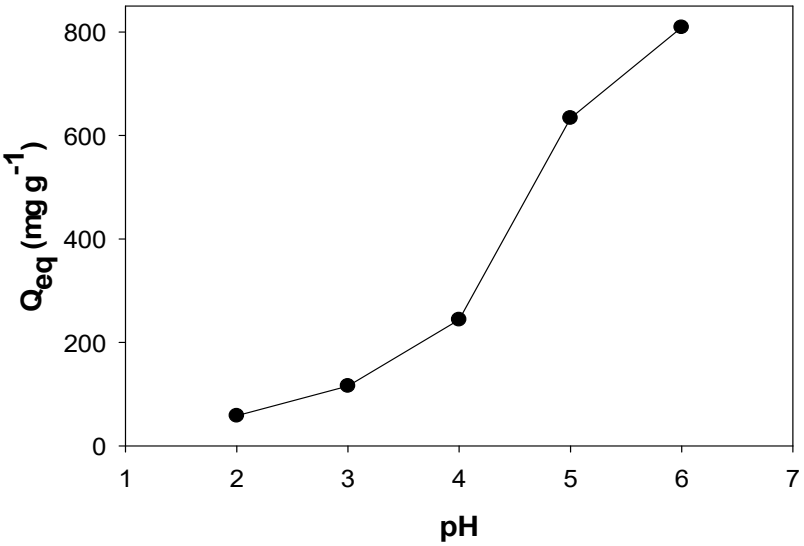

Figure 4. Effects of solution pH to Cu(II) adsorption on PPAC-MS 100.

3.5. Regeneration PPAC-MS 100

A regeneration study of PPAC-MS 100 on Cu(II) removal was conducted using a comparison study of Mg(II) and HCl solution as desorption reagents. PPAC-MS 100 could be regenerated three times, and the final adsorption capacity in the third cycle decreased 40% for Mg(II) solution and 60% for HCl solution in Figure 5. Using Mg(II) solution for the Cu(II) desorption process, competition occurred between Cu(II) and Mg(II) as the main reasons for desorption [53]. Mg(II) tends to replace Cu(II) to form CuO on the surface of absorbents. When using HCl as a desorption reagent, high H^+ concentrations mainly cause metal desorption [54]. PPAC-MS 100 removed Cu(II) three times better than metal desorption reagents, indicating the economic benefits of using a palm-shell waste material.

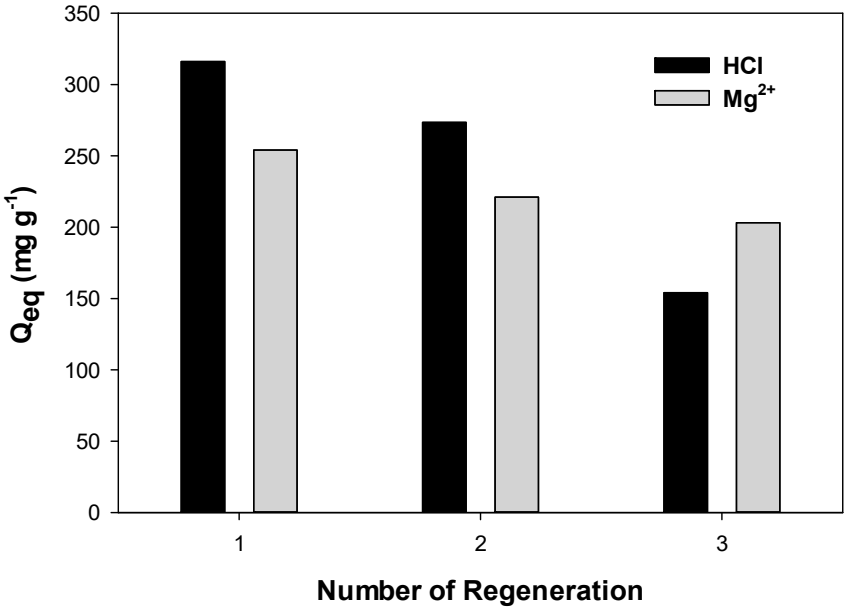

Figure 5. Regeneration of PPAC-MS 100 using Mg^{2+} solution and HCl for three cycles.

3.6. Adsorption Studies on Zn(II), Al(III), Fe(II), Mn(II) and As(V)

PPAC-MS 100 was used to remove five different PTMs in solution, as shown in Figure 6. Table S4 summarizes the Langmuir and Freundlich adsorption constants for dissociated PTMs. PTMs adsorption capacity (mg g^{-1}) for Zn(II), Al(III), Mn (II), Fe(II) and As(V) were 373 mg g^{-1}, 244 mg g^{-1}, 234 mg g^{-1}, 562 mg g^{-1}, and 191 mg g^{-1}, respectively. Overall, the sequence of adsorption capacities of PPAC-MS 100 for different PTMs ion is as follows: Fe(II) > Zn(II) > Al(III) > Mn(II) > As(V). For elements Al(III), Mn(II), Fe (II) and As(V), adsorption data fitted well to Langmuir isotherm, while Zn(II) adsorption fitted well to the Freundlich isotherm. PPAC-MS 100 was efficient in the removal of cation and also anion metal species.

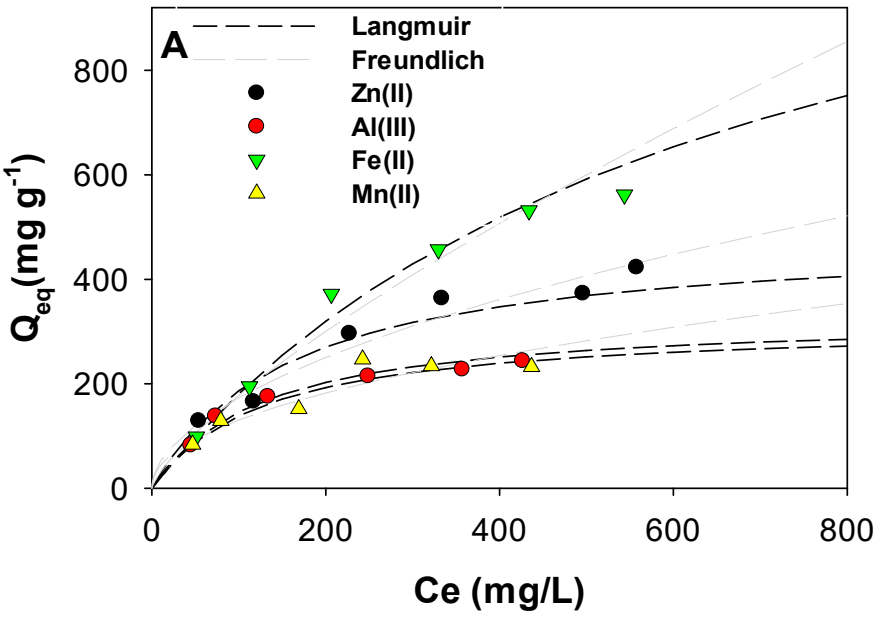

Figure 6. *Cont.*

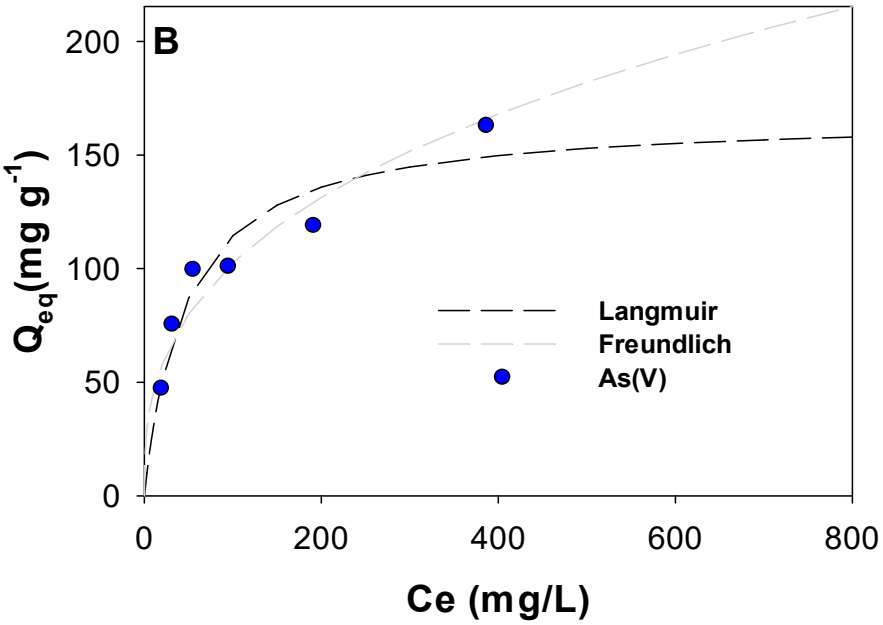

Figure 6. PPAC-MS 100 for (**A**) cation contaminates and (**B**) anion contaminates with Langmuir modeling and Freundlich modeling.

3.7. Copper Removal Mechanisms and Material Characterizations

The removal mechanisms of Cu(II) by PPAC-MS were verified using FTIR, BET, XRD, FESEM-EDS, XRD and XPS. The functional groups of the adsorbents surface were identified through FTIR, as depicted in Figure 7. The main findings are for both the Cu-O band after treatment and Mg-O (or Mg-OH) band in PPAC-MC. The adsorption peaks of Cu-O were observed at 500 cm^{-1} after treatment, indicating the presence of $Cu(OH)_2$ [55]. In PPAC-MS 100, vibration of the Si-O-Si, Mg-OH, and Mg-O groups was observed at peak 1004 cm^{-1} [56], 1410 cm^{-1} [57], and 680 cm^{-1} [58]. The peak of 820 cm^{-1} also proves the existence of Mg-O group [58,59], but this peak may overlap with wide vibration of Si-O-Si at 1004 cm^{-1} [56]. After adsorption onto PPAC-MS 100, the intensity of Si-O-Si bond for PPAC-MS 100 reduced at peak 1004 cm^{-1}, while C-H stretching disappeared, suggesting that the CuO precipitant covered the overall surface. PPAC and PPAC-MS 100 exhibited a broad peak at 3737, 3729 and 3854 cm^{-1} assigned to OH stretching vibration. Additionally, C-H stretching vibration peaks were found at 2924/2853 cm^{-1} on PPAC and PPAC-MS 100 [60]. C=C group and C-O-H group were found at 1556 cm^{-1} and 1448 cm^{-1} on PPAC [61]. After impregnation of $MgSiO_3$ on PPAC, the C-O-H group and C=C bond remain, but are shifted to 1555 cm^{-1} and 1435 cm^{-1}. Overall, the FTIR results verify Cu(II) adsorption by Cu-OH bonding onto the surface of PPAC-MS.

Nitrogen adsorption-desorption isotherms of PPAC-MS 100, PPAC-MS 50, PPAC-MS 25 and PPAC were measured to further illuminate pore characteristics (Figure 8A). The quantity adsorbed volume decreases with the increase of $MgSiO_3$ ratio. This is due to the increase of Mg compound on the surface of PPAC (Figure 9J,K,I). Therefore, an increase in $MgSiO_3$ ratio may enhance the adsorption capacity of Cu(II), but results in the decrease of the adsorbed volume. Because of this phenomenon, it is important to find an optimal ratio between $MgSiO_3$ and PPAC. Based on the International Union of Pure and Applied Chemistry (IUPAC) classification, PPAC, PPAC-MS 25 and PPAC-MS 50 were classified as type I isotherms [28]. The type I isotherms exhibited with a low slope at 0.8–1.0 of p/p^o and characteristics of a highly microporous material. On the other hand, PPAC-MS 100 exhibited significant characteristics of type IV isotherms with a high slope in 0.8–1.0 p/p^o, indicating the filling of the mesopore by capillary condensation [62]. PPAC-MS 100 exhibited an H4 hysteresis loop associated with the parallel line on nitrogen adsorption-desorption curve.

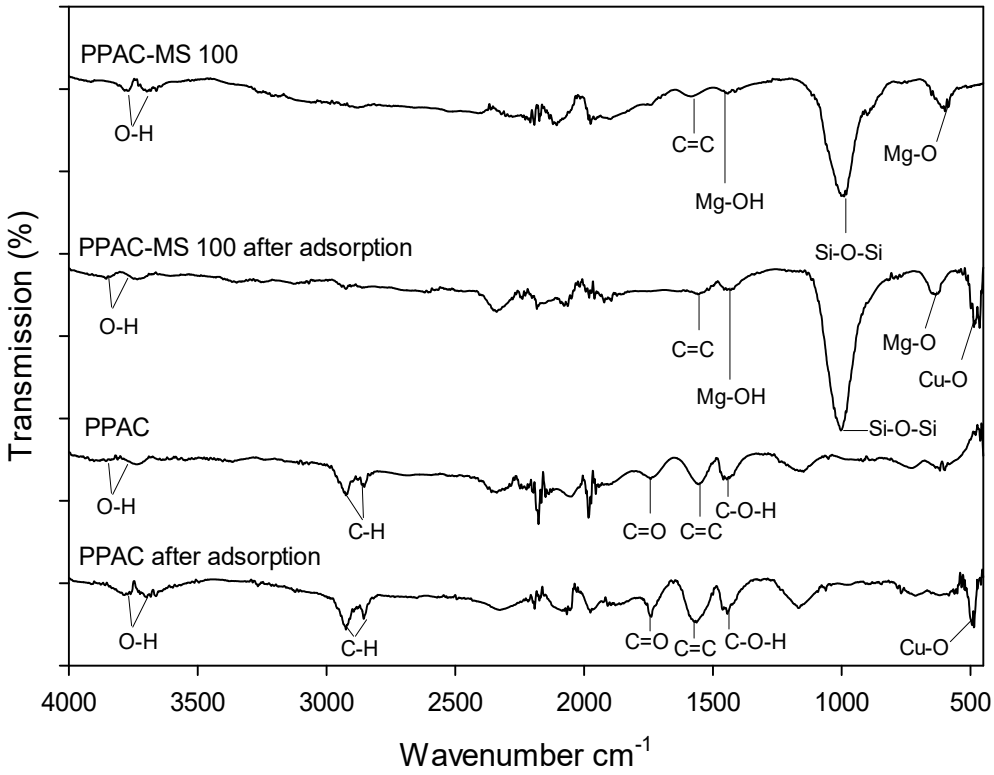

Figure 7. FTIR results of PPAC, PPAC-MS 100, PPAC after adsorption and PPAC-MS 100 after adsorption.

Figure 8B depicts the pore size distribution for PPAC, PPAC-MS25, PPAC-MS 50 and PPAC-MS 100. All adsorbents had a similar peak at 32 Å. $MgSiO_3$ impregnation enhances the mesopore and macropore from at 140–370 Å. Przepiórski, et al. [63] reported carbon material coating with magnesium oxide capable of creating more mesopores under thermal treatment. Table S4 lists the textural characteristics for all absorbents on the total surface area, BET surface area, micropore surface area, total pore volume and micropore volume. $MgSiO_3$ impregnation ratio increased, while the total surface area and BET surface area decreased. The surface textural characteristics are listed in Table S5. Compared to PPAC, average pore width and pore volume increase after $MgSiO_3$ is impregnated. Although the BET surface area and pore volume of modified activated carbon are less than those of PPAC, Cu(II) removal capacity for modified activated carbon is better than PPAC. Thus, the results prove that magnesium silicates play a significant role in Cu(II) removal.

The FESEM images and EDX of PPAC, PPAC-25, PPAC-MS 50 and PPAC-MS 100 were also analyzed (refer Figure 9). The FESEM images illustrate that PPAC exhibited micro and mesopore structure (Figure 9A,B). After $MgSiO_3$ impregnation on PPAC, thin sheet structure form on top of PPAC-MS 100, PPAC-MS 50 and PPAC-MS 25 homogeneously. Interestingly, after impregnation with $MgSiO_3$, the pore structures remained without blocking. FESEM results (Figure 9) reveal the plate-like thin sheet structure formed by interwoven of the $MgSiO_3$ plate within 14 nm diameter. The EDX results show that PPAC-MS 100, PPAC-MS 50 and PPAC-MS 25 had different amounts of Si, Mg, and O compound, which means that $MgSiO_3$ is impregnated on the surface. In another FESEM result (refer Figure 10), the surfaces of PPAC-MS 100 and PPAC became rough and the pores filled with a small crystal plate structure. Compared to PPAC-MS 100, the crystal plate structure is lesser on the surface of PPAC. In the EDX results, Cu and O were detected for both absorbents. Therefore, Cu(II) in solution was successfully removed by adsorption on the surface of PPAC and PPAC-MS 100.

XRD analysis was performed to investigate the chemical compound of PPAC and PPAC-MS 100 before and after adsorption (Figure 11). The XRD pattern suggests that the PPAC sample has asymmetric peaks from 25–50° as indexed to Graphite (ISCD: 88813). Meanwhile, the PPAC-MS shows peaks at 20.07°, 33.39°, 46.4° and 60.14° corresponding to $MgSiO_3$ and peaks at 38.09°, 58.79° and 62.29° (ISCD: 171782) assigned as magnesium hydroxide (ICSD: 34401). SiO_2 was also detected on PPAC-MS 100 at peaks of 24.7° and 58.79°. This result proves that $MgSiO_3$ was successfully impregnated on PPAC after hydrothermal treatment. Compared to PPAC, the graphite peak in PPAC-MS 100 is weak but still extant because the $MgSiO_3$ might not fully occupy PPAC-MS 100. After Cu(II) adsorption, PPAC and PPAC-MS 100 present significant peak at 69.1° and 76.3° assigned as CuO (ISCD: 628614). This proves that the precipitation might involve Cu(II) removal on PPAC and PPAC-MS 100.

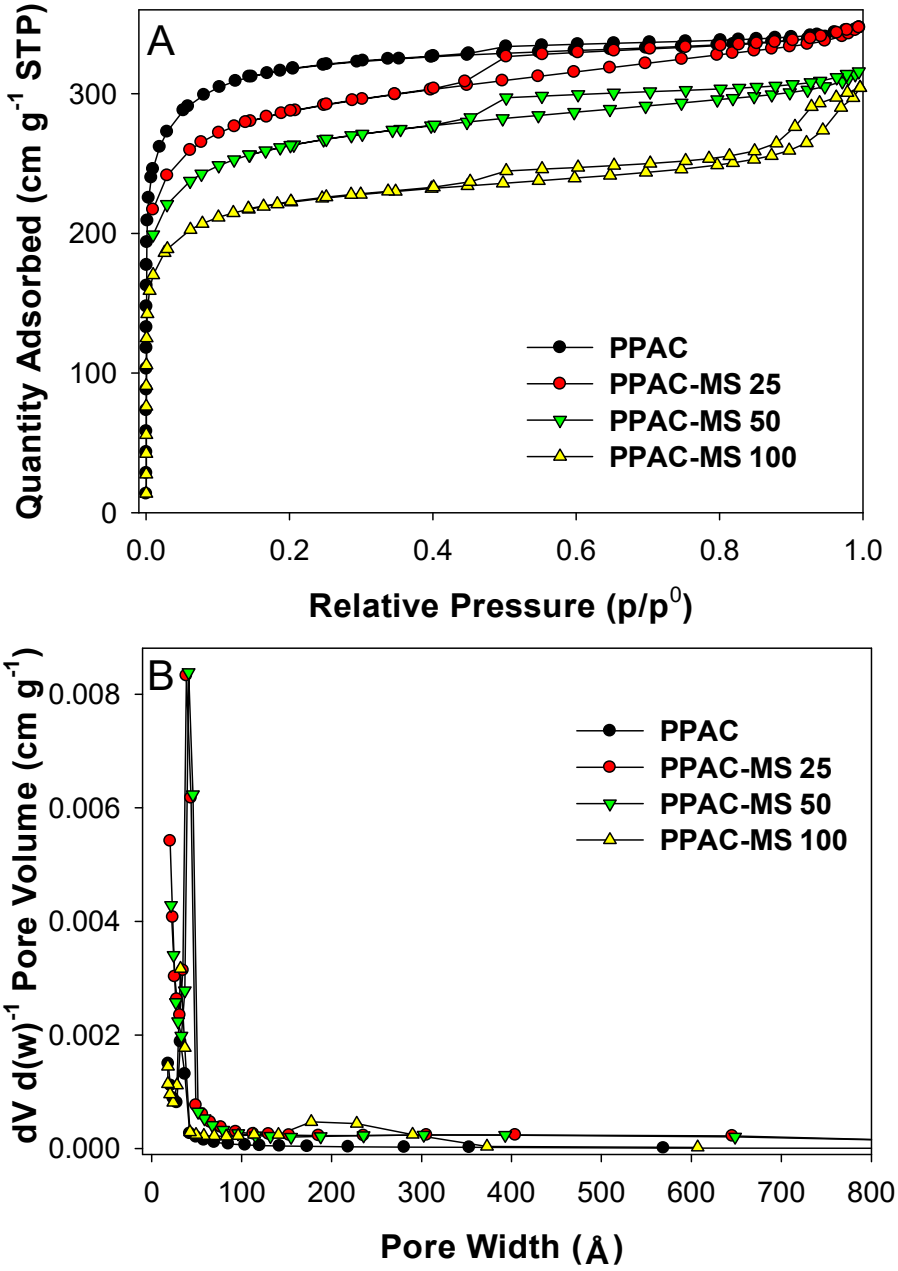

Figure 8. (**A**) N_2 gas adsorption-desorption isotherms of PPAC, PPAC-MS 100, PPAC-MS 50 and pl PPAC-MS 25 and (**B**) differential pore volume vs. pore width.

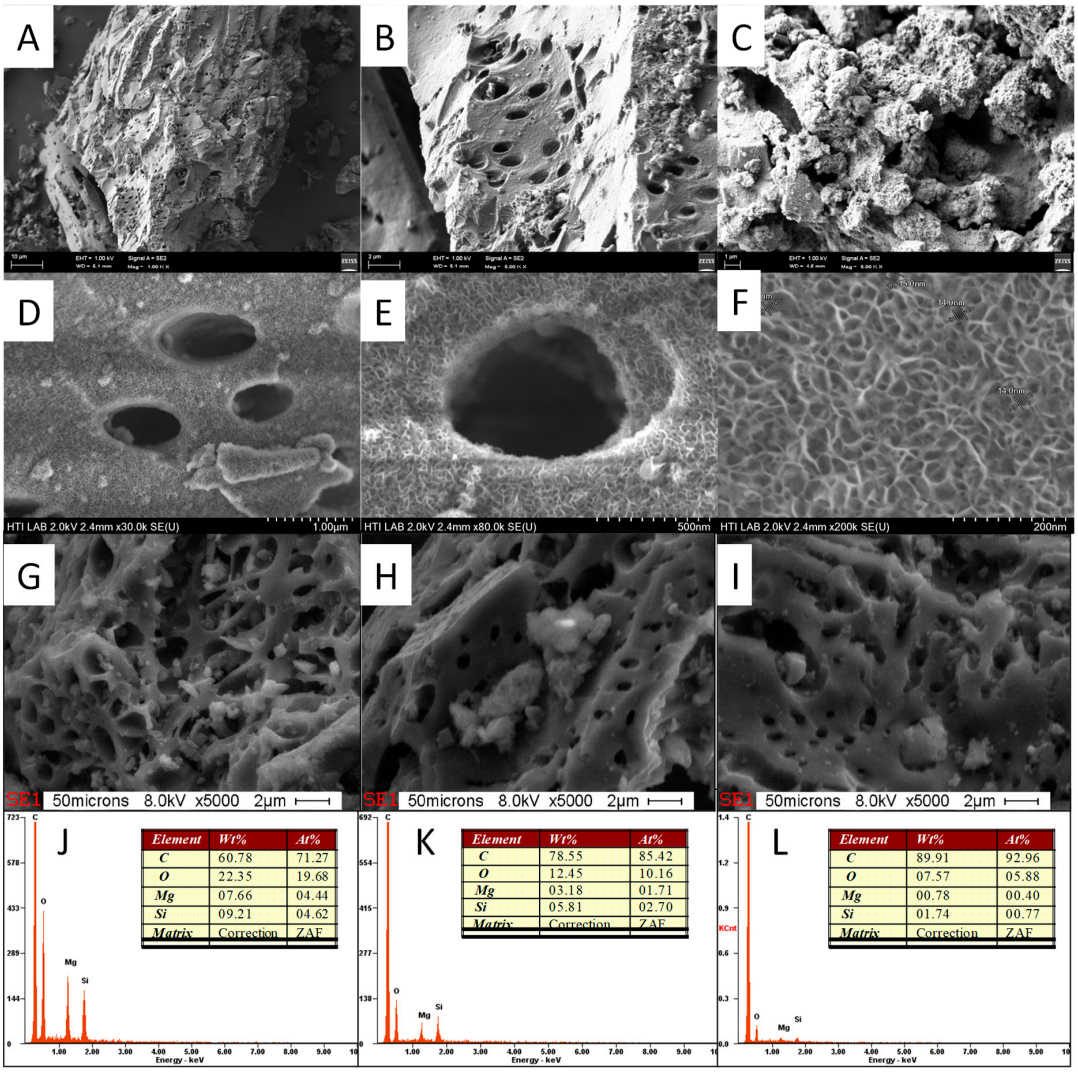

Figure 9. FESEM image of (**A**,**B**) PPAC and (**C**–**F**) PPAC-MS 100, and EDX analysis and its detecting area of (**G**,**J**) PPAC-MS 100, (**H**,**K**) PPAC-MS 50, and (**I**,**L**) PPAC-MS25.

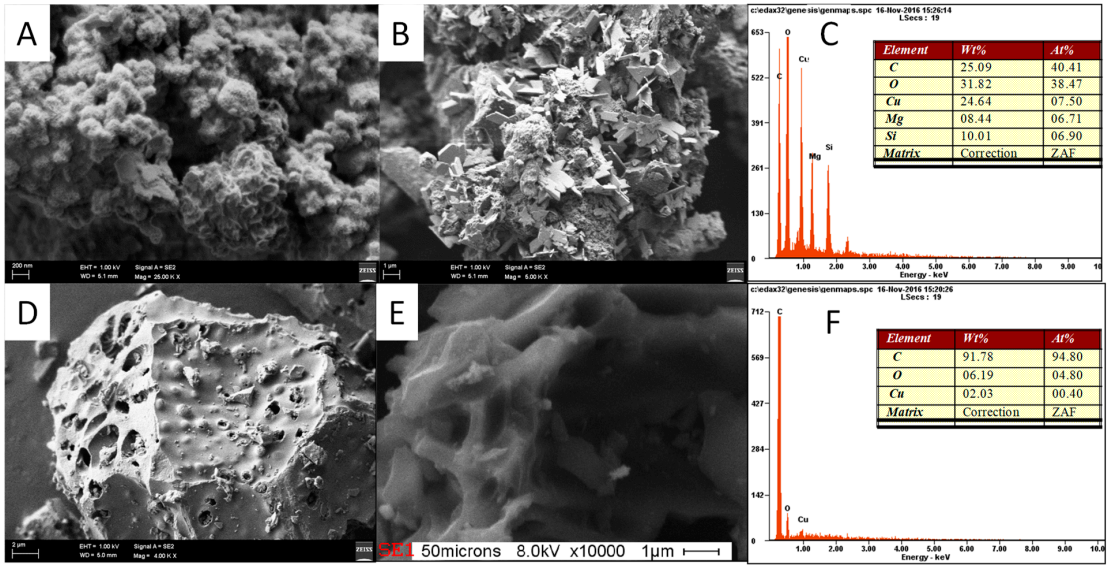

Figure 10. FESEM image after adsorption for (**A**–**C**) PPAC-MS100 and (**D**–**F**) PPAC.

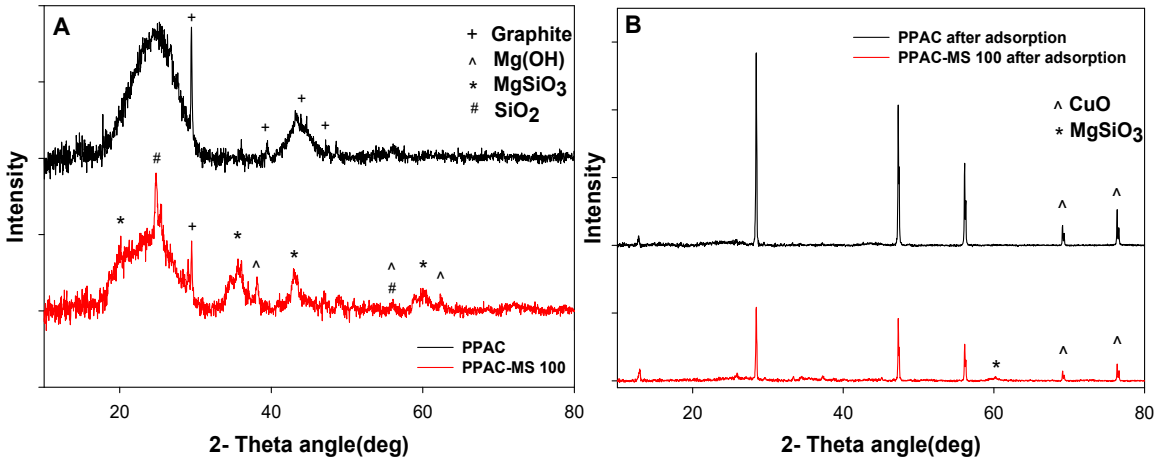

Figure 11. XRD results of PPAC and PPAC-MS 100 (**A**) before adsorption and (**B**) after adsorption.

To understand the electron structure of Cu(II) compound form on PPAC and PPAC-MS 100 after adsorption, Cu core level XPS spectra were studied. Wide scan analysis and Cu core level XPS spectra for PPAC and PPAC-MS 100 are depicted in Figure 12. Wide scan XPS spectrum of PPAC indicates O, C and Cu existence while Si, O, Cu, Mg existence on PPAC-MS 100. As shown in Figure 12 the peaks at 935 eV and 953 eV and 937 eV and 955 eV are associated with the binding energy of Cu $2p^{3/2}$ and Cu $2p^{1/2}$ for PPAC and PPAC-MS 100. A Cu component with low binding energy of Cu $2p^{3/2}$ can be assigned as a tetracoordinated Cu(I) ion species, while PPAC-MS 100 and PPAC Cu component can be assigned as an acta coordinated Cu(II) ion species because the Cu $2p^{3/2}$ for PPAC-MS 100 and PPAC is located above 935 eV [64]. Bivalent CuO was also observed on PPAC and PPAC-MS 100 (Figure S1 at SI). Therefore, it is proven that CuO was formed on the PPAC and PPAC-MS 100 surface. Moreover, a satellite peak appeared at the Cu core level XPS spectra for both PPAC and PPAC-MS 100. The appearance of the satellite peak indicates that CuO has a d9 configuration in a ground state between Cu $2p^{3/2}$ and Cu $2p^{1/2}$ peak [65].

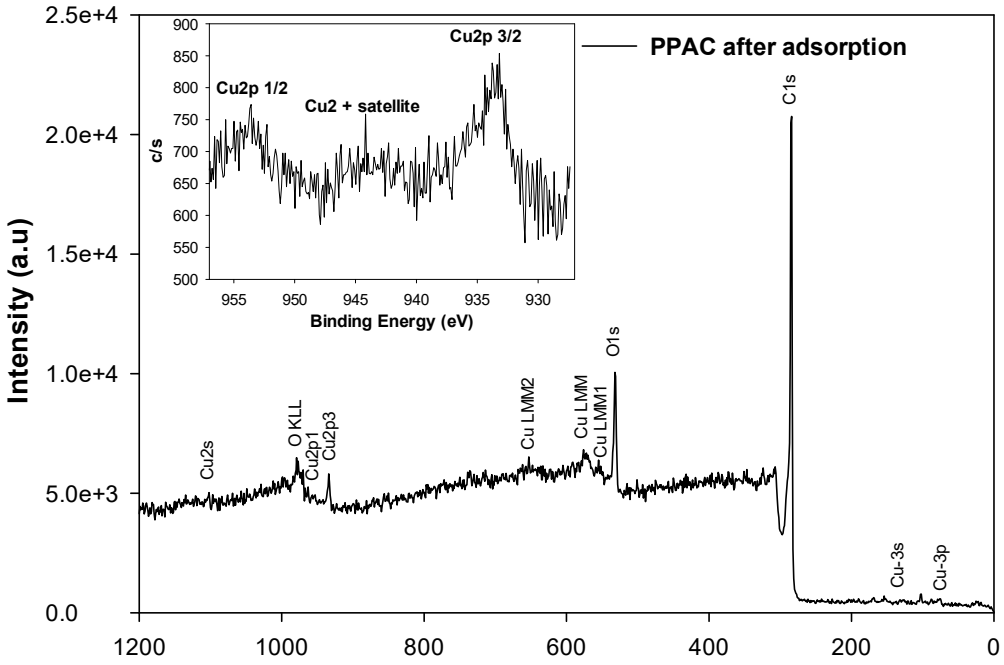

Figure 12. *Cont.*

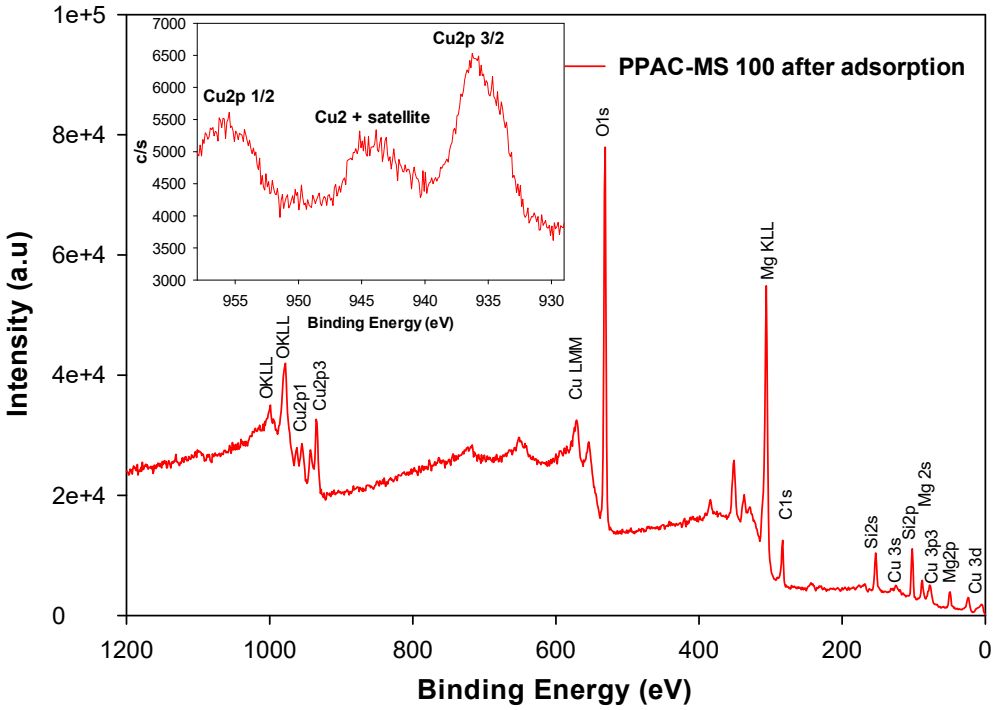

Figure 12. XPS wide scan analysis for PPAC and PPAC-MS 100 after adsorption.

Based on the characterization of materials, Cu(II) removal can be proposed as adsorption together with ion-exchange and precipitation for PPAC-MS 100. First, dissolution of $Mg(OH)_2$ releases hydroxide and Mg(II) ions to the surface of impregnated PPAC-MS 100 caused the pH of solution increases. Thus, Cu(II) may form precipitation at this stage. Results for XPS and XRD have sufficient agreement to support the observation that CuO component was precipitated and adsorbed on PPAC-MS 100. Second, ion exchange can occur between Mg and Cu ions on the absorbent surface. Thus, the mechanism of Cu(II) removal by PPAC-MS can be considered adsorption together with precipitation and ion-exchange. The adsorption of Cu(II) ion on PPAC is strongly influenced by the pH of the solution. PPAC is activated by KOH, OH^- release and increased pH, resulting in precipitation. Additionally, the negatively charged C-O group can attract positively charged Cu(II) ions in adsorption as detected on PPAC through FTIR analysis.

4. Conclusions

PPAC impregnated with $MgSiO_3$ was prepared using mild hydrothermal treatment and exhibited good Cu(II) removal. A porous structure remained after $MgSiO_3$ impregnation on PPAC, forming a thin layer sheet structure as observed via FESEM. The PPAC, PPAC-MS25 and PPAC-MS50 isotherm data fitted well with Langmuir isotherm model with the Cu(II) removal capacity of 165 mg g^{-1}, 220 mg g^{-1}, 285 mg g^{-1}. The highest Cu(II) adsorption capacity of 369 mg g^{-1} for PPAC-MS 100 fitted well with the Freundlich isotherm model. Pseudo 2nd order fitted well to all kinetic adsorption data, describing a chemisorption-dominated adsorption process. Kinetic data revealed that Cu(II) adsorption capacity decreased when ionic strength concentration increased. Additionally, an increase in ionic strength resulted in a Cu(II) sorption rate increase. PPAC-MS 100 regenerated using HCl and Mg^{2+} solution exhibited a good result on Cu(II) removal for three cycles. As an absorbent, PPAC-MS100 has a strong affinity for the removal of Zn(II), Al(III), Fe(II), Mn(II), and As(V), with adsorption capacities of 373 mg g^{-1}, 244 mg g^{-1}, 234 mg g^{-1}, 562 mg g^{-1}, and 191 mg g^{-1}, respectively. Therefore, PPAC-MS 100 is a promising high-efficiency absorbent for wastewater treatment.

Supplementary Materials: The following are available at http://www.mdpi.com/2075-4701/8/10/741/s1, Table S1. Modeling of isotherm result for PPAC, PPAC-MS 25, PPAC-MS 50, and PPAC-MS 100; Table S2. Comparison of Cu(II) adsorption capacities between PPAC, PPAC-MS 100 and other absorbents; Table S3. Modeling of Kinetic result for PPAC, PPAC-MS 25, PPAC-MS 50 and PPAC-MS 100; Table S4. Isotherm result for PPAC-MS 100 for As, Zn, Al, Fe and Mn removal; Table S5. Pore characteristic of PPAC, PPAC-MS 25, PPAC-MS 50, and PPAC-MS 100 and Figure S1. XPS analysis binding energy after adsorption (A) PPAC-MS 100 and (B) PPAC.

Author Contributions: Conceptualization, C.E.C.; Writing-Original Draft Preparation, C.E.C.; Writing-Review & Editing, G.L. and M.J.; Supervision, C.M.P. and S.I.; Funding Acquisition, S.I. and C.M.P.

Acknowledgments: This work was supported by Postgraduate Research Grant (PPP) (PG210-2015B) and Basic Science Research Program through the National Research Foundation of Korea (NRF) funded by the Ministry of Education (NRF-2018R1A6A1A03024962).

Conflicts of Interest: The authors declare no conflict of interest.

References

1. Meers, E.; Ruttens, A.; Hopgood, M.J.; Samson, D.; Tack, F.M.G. Comparison of edta and edds as potential soil amendments for enhanced phytoextraction of heavy metals. *Chemosphere* **2005**, *58*, 1011–1022. [CrossRef] [PubMed]
2. Smallwood, R.A.; Williams, H.A.; Rosenoer, V.M.; Sherlock, S. Liver-copper levels in liver disease: Studies using neurtron activation analysis. *Lancet* **1968**, *292*, 1310–1313. [CrossRef]
3. Yang, X.; Li, Q.; Tang, Z.; Zhang, W.; Yu, G.; Shen, Q.; Zhao, F.-J. Heavy metal concentrations and arsenic speciation in animal manure composts in China. *Waste Manag.* **2017**, *64*, 333–339. [CrossRef] [PubMed]
4. Madzin, Z.; Shai-in, M.F.; Kusin, F.M. Comparing heavy metal mobility in active and abandoned mining sites at bestari jaya, selangor. *Procedia Environ. Sci.* **2015**, *30*, 232–237. [CrossRef]
5. Dąbrowski, A.; Hubicki, Z.; Podkościelny, P.; Robens, E. Selective removal of the heavy metal ions from waters and industrial wastewaters by ion-exchange method. *Chemosphere* **2004**, *56*, 91–106. [CrossRef] [PubMed]
6. Mobasherpour, I.; Salahi, E.; Ebrahimi, M. Thermodynamics and kinetics of adsorption of Cu(ii) from aqueous solutions onto multi-walled carbon nanotubes. *J. Saudi Chem. Soc.* **2014**, *18*, 792–801. [CrossRef]
7. Barakat, M.A. New trends in removing heavy metals from industrial wastewater. *Arab. J. Chem.* **2011**, *4*, 361–377. [CrossRef]
8. Babel, S.; Kurniawan, T.A. Low-cost adsorbents for heavy metals uptake from contaminated water: A review. *J. Hazard. Mater.* **2003**, *97*, 219–243. [CrossRef]
9. Furlan, F.R.; de Melo da Silva, L.G.; Morgado, A.F.; de Souza, A.A.U.; Guelli Ulson de Souza, S.M.A. Removal of reactive dyes from aqueous solutions using combined coagulation/flocculation and adsorption on activated carbon. *Resour. Conserv. Recycl.* **2010**, *54*, 283–290. [CrossRef]
10. Kyzas, G.Z.; Deliyanni, E.A.; Bikiaris, D.N.; Mitropoulos, A.C. Graphene composites as dye adsorbents: Review. *Chem. Eng. Res. Des.* **2018**, *129*, 75–88. [CrossRef]
11. Fan, T.-T.; Wang, Y.-J.; Li, C.-B.; He, J.-Z.; Gao, J.; Zhou, D.-M.; Friedman, S.P.; Sparks, D.L. Effect of organic matter on sorption of zn on soil: Elucidation by wien effect measurements and exafs spectroscopy. *Environ. Sci. Technol.* **2016**, *50*, 2931–2937. [CrossRef] [PubMed]
12. Linares, N.; Silvestre-Albero, A.M.; Serrano, E.; Silvestre-Albero, J.; Garcia-Martinez, J. Mesoporous materials for clean energy technologies. *Chem. Soc. Rev.* **2014**, *43*, 7681–7717. [CrossRef] [PubMed]
13. Lua, A.C.; Guo, J. Microporous oil-palm-shell activated carbon prepared by physical activation for gas-phase adsorption. *Langmuir* **2001**, *17*, 7112–7117. [CrossRef]
14. Tsai, W.T.; Chang, C.Y.; Wang, S.Y.; Chang, C.F.; Chien, S.F.; Sun, H.F. Cleaner production of carbon adsorbents by utilizing agricultural waste corn cob. *Resour. Conserv. Recycl.* **2001**, *32*, 43–53. [CrossRef]
15. Yantasee, W.; Lin, Y.; Fryxell, G.E.; Alford, K.L.; Busche, B.J.; Johnson, C.D. Selective removal of copper(ii) from aqueous solutions using fine-grained activated carbon functionalized with amine. *Ind. Eng. Chem. Res.* **2004**, *43*, 2759–2764. [CrossRef]
16. Mahaninia, M.H.; Rahimian, P.; Kaghazchi, T. Modified activated carbons with amino groups and their copper adsorption properties in aqueous solution. *Chin. J. Chem. Eng.* **2015**, *23*, 50–56. [CrossRef]

17. Reza, R.A.; Ahmaruzzaman, M. A novel synthesis of Fe_2O_3@activated carbon composite and its exploitation for the elimination of carcinogenic textile dye from an aqueous phase. *RSC Adv.* **2015**, *5*, 10575–10586. [CrossRef]
18. Mahdavi, S.; Jalali, M.; Afkhami, A. Removal of heavy metals from aqueous solutions using Fe_3O_4, ZnO, and CuO nanoparticles. *J. Nanopart. Res.* **2012**, *14*, 846. [CrossRef]
19. Ahn, C.K.; Park, D.; Woo, S.H.; Park, J.M. Removal of cationic heavy metal from aqueous solution by activated carbon impregnated with anionic surfactants. *J. Hazard. Mater.* **2009**, *164*, 1130–1136. [CrossRef] [PubMed]
20. Seymour, M.B.; Su, C.; Gao, Y.; Lu, Y.; Li, Y. Characterization of carbon nano-onions for heavy metal ion remediation. *J. Nanopart. Res.* **2012**, *14*, 1087. [CrossRef]
21. Liao, P.; Yuan, S.; Zhang, W.; Tong, M.; Wang, K. Mechanistic aspects of nitrogen-heterocyclic compound adsorption on bamboo charcoal. *J. Colloid Interface Sci.* **2012**, *382*, 74–81. [CrossRef] [PubMed]
22. Lo, S.-F.; Wang, S.-Y.; Tsai, M.-J.; Lin, L.-D. Adsorption capacity and removal efficiency of heavy metal ions by moso and ma bamboo activated carbons. *Chem. Eng. Res. Des.* **2012**, *90*, 1397–1406. [CrossRef]
23. Wong, S.; Lee, Y.; Ngadi, N.; Inuwa, I.M.; Mohamed, N.B. Synthesis of activated carbon from spent tea leaves for aspirin removal. *Chin. J. Chem. Eng.* **2018**, *26*, 1003–1011. [CrossRef]
24. Shukla, S.R.; Pai, R.S. Adsorption of Cu(ii), Ni(ii) and Zn(ii) on dye loaded groundnut shells and sawdust. *Sep. Purif. Technol.* **2005**, *43*, 1–8. [CrossRef]
25. Lalhmunsiama; Lee, S.M.; Choi, S.S.; Tiwari, D. Simultaneous removal of Hg(ii) and phenol using functionalized activated carbon derived from areca nut waste. *Metals* **2017**, *7*, 248. [CrossRef]
26. Hameed, B.H.; El-Khaiary, M.I. Malachite green adsorption by rattan sawdust: Isotherm, kinetic and mechanism modeling. *J. Hazard. Mater.* **2008**, *159*, 574–579. [CrossRef] [PubMed]
27. Sathishkumar, M.; Binupriya, A.R.; Kavitha, D.; Selvakumar, R.; Sheema, K.K.; Choi, J.G.; Yun, S.E. Organic micro-pollutant removal in liquid-phase using carbonized silk cotton hull. *J. Environ. Sci.* **2008**, *20*, 1046–1054. [CrossRef]
28. Jais, F.M.; Ibrahim, S.; Yoon, Y.; Jang, M. Enhanced arsenate removal by lanthanum and nano–magnetite composite incorporated palm shell waste–based activated carbon. *Sep. Purif. Technol.* **2016**, *169*, 93–102. [CrossRef]
29. Yu, Y.; Hu, Z.; Chen, Z.; Yang, J.; Gao, H.; Chen, Z. Organically-modified magnesium silicate nanocomposites for high-performance heavy metal removal. *RSC Adv.* **2016**, *6*, 97523–97531. [CrossRef]
30. Lu, H.; Wang, J.; Stoller, M.; Wang, T.; Bao, Y.; Hao, H. An overview of nanomaterials for water and wastewater treatment. *Adv. Mater. Sci. Eng.* **2016**, *2016*, 4964828. [CrossRef]
31. Brar, S.K.; Verma, M.; Tyagi, R.D.; Surampalli, R.Y. Engineered nanoparticles in wastewater and wastewater sludge—Evidence and impacts. *Waste Manag.* **2010**, *30*, 504–520. [CrossRef] [PubMed]
32. Mahmoud, M.E.; Khalifa, M.A.; El Wakeel, Y.M.; Header, M.S.; Abdel-Fattah, T.M. Engineered nano-magnetic iron oxide-urea-activated carbon nanolayer sorbent for potential removal of uranium (vi) from aqueous solution. *J. Nucl. Mater.* **2017**, *487*, 13–22. [CrossRef]
33. Karnib, M.; Kabbani, A.; Holail, H.; Olama, Z. Heavy metals removal using activated carbon, silica and silica activated carbon composite. *Energy Procedia* **2014**, *50*, 113–120. [CrossRef]
34. Wang, M.C.; Sheng, G.D.; Qiu, Y.P. A novel manganese-oxide/biochar composite for efficient removal of lead(ii) from aqueous solutions. *Int. J. Environ. Sci. Technol.* **2015**, *12*, 1719–1726. [CrossRef]
35. Gaya, U.I.; Otene, E.; Abdullah, A.H. Adsorption of aqueous Cd(ii) and Pb(ii) on activated carbon nanopores prepared by chemical activation of doum palm shell. *Springerplus* **2015**, *4*, 458. [CrossRef] [PubMed]
36. Choong, C.E.; Ibrahim, S.; Yoon, Y.; Jang, M. Removal of lead and bisphenol a using magnesium silicate impregnated palm-shell waste powdered activated carbon: Comparative studies on single and binary pollutant adsorption. *Ecotoxicol. Environ. Saf.* **2018**, *148*, 142–151. [CrossRef] [PubMed]
37. St. Vassileva, P.; Detcheva, A.K. Adsorption of some transition metal ions [Cu(ii), Fe(iii), Cr(iii) and Au(iii)] onto lignite-based activated carbons modified by oxidation. *Adsorpt. Sci. Technol.* **2010**, *28*, 229–242.
38. ASTM. Astm d1976-18. In *Standard Test Method for Elements in Water by Inductively-Coupled Plasma Atomic Emission Spectroscopy*; ASTM International: West Conshohocken, PA, USA, 2018.
39. Zhan, W.; Xu, C.; Qian, G.; Huang, G.; Tang, X.; Lin, B. Adsorption of Cu(ii), Zn(ii), and Pb(ii) from aqueous single and binary metal solutions by regenerated cellulose and sodium alginate chemically modified with polyethyleneimine. *RSC Adv.* **2018**, *8*, 18723–18733. [CrossRef]

40. Anastopoulos, I.; Karamesouti, M.; Mitropoulos, A.C.; Kyzas, G.Z. A review for coffee adsorbents. *J. Mol. Liq.* **2017**, *229*, 555–565. [CrossRef]
41. Rafiq, Z.; Nazir, R.; Shah, M.R.; Ali, S. Utilization of magnesium and zinc oxide nano-adsorbents as potential materials for treatment of copper electroplating industry wastewater. *J. Environ. Chem. Eng.* **2014**, *2*, 642–651. [CrossRef]
42. Zhang, K.; Li, H.; Xu, X.; Yu, H. Facile and efficient synthesis of nitrogen-functionalized graphene oxide as a copper adsorbent and its application. *Ind. Eng. Chem. Res.* **2016**, *55*, 2328–2335. [CrossRef]
43. Wang, P.; Ye, Y.; Liang, D.; Sun, H.; Liu, J.; Tian, Z.; Liang, C. Layered mesoporous $Mg(OH)_2$/GO nanosheet composite for efficient removal of water contaminants. *RSC Adv.* **2016**, *6*, 26977–26983. [CrossRef]
44. Kadirvelu, K.; Faur-Brasquet, C.; Cloirec, P.L. Removal of Cu(ii), Pb(ii), and Ni(ii) by adsorption onto activated carbon cloths. *Langmuir* **2000**, *16*, 8404–8409. [CrossRef]
45. Khodaie, M.; Ghasemi, N.; Moradi, B.; Rahimi, M. Removal of methylene blue from wastewater by adsorption onto $ZnCl_2$ activated corn husk carbon equilibrium studies. *J. Chem.* **2013**, *2013*, 383985. [CrossRef]
46. Langmuir, I. The adsorption of gases on plane surfaces of glass, mica and platinum. *J. Am. Chem. Soc.* **1918**, *40*, 1361–1403. [CrossRef]
47. Freundlich, H.M.F. Over the adsorption in solution. *J. Phys. Chem.* **1906**, *57*, 385–471.
48. ElShafei, G.M.S.; ElSherbiny, I.M.A.; Darwish, A.S.; Philip, C.A. Silkworms' feces-based activated carbons as cheap adsorbents for removal of cadmium and methylene blue from aqueous solutions. *Chem. Eng. Res. Des.* **2014**, *92*, 461–470. [CrossRef]
49. Yakout, S.M.; Borai, E.H. Adsorption behavior of cadmium onto natural chabazite: Batch and column investigations. *Desalination Water Treat.* **2014**, *52*, 4212–4222. [CrossRef]
50. Xu, J.; Wang, L.; Zhu, Y. Decontamination of bisphenol a from aqueous solution by graphene adsorption. *Langmuir* **2012**, *28*, 8418–8425. [CrossRef] [PubMed]
51. Nouri, L.; Ghodbane, I.; Hamdaoui, O.; Chiha, M. Batch sorption dynamics and equilibrium for the removal of cadmium ions from aqueous phase using wheat bran. *J. Hazard. Mater.* **2007**, *149*, 115–125. [CrossRef] [PubMed]
52. Johnson, P.D.; Watson, M.A.; Brown, J.; Jefcoat, I.A. Peanut hull pellets as a single use sorbent for the capture of Cu(ii) from wastewater. *Waste Manag.* **2002**, *22*, 471–480. [CrossRef]
53. Ou, Q.; Zhou, L.; Zhao, S.; Geng, H.; Hao, J.; Xu, Y.; Chen, H.; Chen, X. Self-templated synthesis of bifunctional Fe_3O_4@$MgSiO_3$ magnetic sub-microspheres for toxic metal ions removal. *Chem. Eng. J.* **2012**, *180*, 121–127. [CrossRef]
54. Sharma, Y.C.; Srivastava, V.; Singh, V.K.; Kaul, S.N.; Weng, C.H. Nano-adsorbents for the removal of metallic pollutants from water and wastewater. *Environ. Technol.* **2009**, *30*, 583–609. [CrossRef] [PubMed]
55. Zhang, Y.X.; Huang, M.; Li, F.; Wen, Z.Q. Controlled synthesis of hierarchical cuo nanostructures for electrochemical capacitor electrodes. *Int. J. Electrochem. Sci.* **2013**, *8*, 8645–8661.
56. Tao, Q.; Zhu, J.; Frost, R.L.; Bostrom, T.E.; Wellard, R.M.; Wei, J.; Yuan, P.; He, H. Silylation of layered double hydroxides via a calcination–rehydration route. *Langmuir* **2010**, *26*, 2769–2773. [CrossRef] [PubMed]
57. Cao, H.; Zheng, H.; Yin, J.; Lu, Y.; Wu, S.; Wu, X.; Li, B. $Mg(OH)_2$ complex nanostructures with superhydrophobicity and flame retardant effects. *J. Phys. Chem. C* **2010**, *114*, 17362–17368. [CrossRef]
58. Dhaouadi, H.; Chaabane, H.; Touati, F. $Mg(OH)_2$ nanorods synthesized by a facile hydrothermal method in the presence of ctab. *Nano-Micro Lett.* **2011**, *3*, 153–159. [CrossRef]
59. Pei, L.-Z.; Yin, W.-Y.; Wang, J.-F.; Chen, J.; Fan, C.-G.; Zhang, Q.-F. Low temperature synthesis of magnesium oxide and spinel powders by a sol-gel process. *Mater. Res.* **2010**, *13*, 339–343. [CrossRef]
60. Viana, R.B.; da Silva, A.B.F.; Pimentel, A.S. Infrared spectroscopy of anionic, cationic, and zwitterionic surfactants. *Adv. Chem. Phys.* **2012**, *2012*, 903272. [CrossRef]
61. Barth, A. Infrared spectroscopy of proteins. *Biochim. Biophys. Acta* **2007**, *1767*, 1073–1101. [CrossRef] [PubMed]
62. Wang, K.; Zhao, J.; Li, H.; Zhang, X.; Shi, H. Removal of cadmium(ii) from aqueous solution by granular activated carbon supported magnesium hydroxide. *J. Taiwan Inst. Chem. Eng.* **2016**, *61*, 287–291. [CrossRef]
63. Przepiórski, J.; Czyżewski, A.; Pietrzak, R.; Tryba, B. MgO/CaO-loaded porous carbons for carbon dioxide capture. *J. Therm. Anal. Calorim.* **2013**, *111*, 357–364. [CrossRef]

64. Li, B.; Luo, X.; Zhu, Y.; Wang, X. Immobilization of Cu(ii) in kit-6 supported Co_3O_4 and catalytic performance for epoxidation of styrene. *Appl. Surf. Sci.* **2015**, *359*, 609–620. [CrossRef]
65. Hu, L.; Shi, L.; Hong, H.; Li, M.; Bao, Q.; Tang, J.; Ge, J.; Lu, J.; Cao, X.; Gu, H. Catalytic epoxidation of stilbene with FePt@Cu nanowires and molecular oxygen. *Chem. Commun.* **2010**, *46*, 8591–8593. [CrossRef] [PubMed]